A peptide of a type I toxin-antitoxin system induces *Helicobacter pylori* morphological transformation from spiral-shape to coccoids

Short title: *H. pylori* shape conversion induced by a TA toxin

Lamya El Mortaji [1], Stéphanie Marsin [2+], Aline Rifflet [3,4], Ivo G. Boneca [3,4], J. Pablo Radicella [2], Gérard Péhau-Arnaudet [5] and Hilde De Reuse [1] *

[1] Institut Pasteur, Département de Microbiologie, Unité Pathogenèse de *Helicobacter*, ERL CNRS 6002, 28 rue du Dr Roux 75724 PARIS Cedex 15 FRANCE.

[2] CEA, Institute of Molecular and Cellular Radiobiology, Institut François Jacob, INSERM UMR967, Universités Paris Diderot et Paris Sud, Fontenay-aux-Roses, France.

+ Current affiliation: I2BC/UMR 9198 CNRS- CEA -Université Paris Sud, Bat. 430, Orsay, FRANCE.

[3] Institut Pasteur, Département de Microbiologie, Unité Biologie et Génétique de la Paroi Bactérienne, 75724 PARIS, FRANCE.

[4] INSERM, Equipe Avenir, 75015 Paris, France

[5] Institut Pasteur, Ultrastructural BioImaging (*UTechS* UBI) /UMR CNRS 3528, PARIS, FRANCE.

* -Corresponding author: Hilde De Reuse (hdereuse@pasteur.fr)

Institut Pasteur, Unité Pathogenèse de *Helicobacter*

28, rue du Docteur Roux

75724 PARIS Cedex 15 FRANCE

Tel : +33 1 40 61 36 41

Summary

Toxin-antitoxin systems are found in many bacterial chromosomes and plasmids with roles ranging from plasmid stabilization to biofilm formation and persistence. In these systems, the expression/activity of the toxin is counteracted by an antitoxin, which in type I systems is an antisense-RNA. While the regulatory mechanisms of these systems are mostly well-defined, the toxins' biological activity and expression conditions are less understood. Here, these questions were investigated with a type I toxin-antitoxin system (AapA1-IsoA1) expressed from the chromosome of the major human pathogen *Helicobacter pylori*. We show that expression of the AapA1 toxin in *H. pylori* causes growth arrest associated with massive morphological transformation from spiral-shaped bacteria to round coccoid cells. Coccoids are observed in patients and during *in vitro* growth as a response to different conditions such as oxidative stress. The AapA1 toxin, first molecular effector of coccoids to be identified, targets *H. pylori* inner membrane without disruption, as visualized by Cryo-EM. The peptidoglycan composition of coccoids is modified as compared to spiral bacteria. No major changes in membrane potential or ATP concentration result from AapA1 expression, suggesting coccoid viability. Using single-cell live microscopy, we observed that shape conversion is associated with cell division interference. Oxidative stress represses antitoxin promoter activity and enhances processing of its transcript leading to an imbalanced ratio in favor of AapA1 toxin expression.

Our data are in favor of viable coccoids with characteristics of dormant bacteria that might be important in *H. pylori* infections refractory to treatment.

49 **Significance Statement**

50 *Helicobacter pylori*, a gastric pathogen responsible for 800,000 deaths in the world every
51 year, is encountered, both *in vitro* and in patients, as spiral-shaped bacteria and as round cells
52 named coccoids. We discovered that the toxin from a chromosomal type I toxin-antitoxin
53 system is targeting *H. pylori* membrane and acting as an effector of the morphological
54 conversion of *H. pylori* to coccoids. We showed that these round cells maintain their
55 membrane integrity and metabolism, strongly suggesting that they are viable dormant bacteria.
56 Oxidative stress was identified as a signal inducing toxin expression. Our findings reveal new
57 insights into a form of dormancy of this bacterium that might be associated with *H. pylori*
58 infections refractory to treatment.

59

60

61 **Introduction**

62 Toxin-antitoxin (TA) systems are small genetic elements that are widely distributed on
63 bacterial mobile genetic elements and among archaeal and bacterial genomes, often in
64 multiple copies (1-3). They code for a small stable toxic protein, designated toxin, whose
65 action or expression is counteracted by an unstable antitoxin molecule that can either be an
66 RNA or a protein (3, 4). Under conditions in which the toxins can act, they target essential
67 cellular processes or components (transcription, DNA replication, translation, cell wall or
68 membrane) resulting in growth arrest or cell death (3, 4). The molecular mechanism of the
69 toxins' activities and their regulation are often known in detail while the biological function
70 remains elusive. TA systems take part in plasmid maintenance and protection from phage
71 infection. Less is known on the biological functions and targets of the chromosomally
72 encoded TA systems. Some are important for bacterial survival in their mammalian host (5)
73 or biofilm formation (6). There is accumulating evidence that upon stress conditions, some
74 TA systems play a role in the switch of actively growing bacteria to persisters or dormant
75 cells (7, 8). Persister bacteria constitute a subpopulation that is metabolically active but slow-
76 growing and highly tolerant to antibiotics and stress conditions (9). Persistence is considered
77 as an important cause of recalcitrance of chronic bacterial infections to therapy. However,
78 stress-induced activation of TA-encoded toxins does not necessarily cause persister formation
79 (10) and it was more generally found that decreased intracellular ATP concentration is a
80 landmark of persister formation (11).

81 In the present work, we explored the role of TA systems in *Helicobacter pylori*, a
82 bacterium that colonizes the stomach of half of the human population worldwide and causes
83 the development of gastritis. In some cases, gastritis evolves into peptic ulcer disease or
84 gastric carcinoma that causes about 800,000 deaths in the world every year (12, 13). This
85 microaerophilic bacterium is unique in its capacity to persistently colonize the stomach
86 despite its extreme acidity and intense immune response (13). The molecular mechanisms at

87 the origin of this exceptional adaptation capacity of *H. pylori* remain only partially
88 understood and their elucidation is crucial to understand its virulence and to improve its
89 eradication in patients with recurrent peptic ulcer disease. *H. pylori* is a Gram-negative
90 bacterium with a helical shape. Upon stress conditions (antibiotics, aerobic growth) or
91 prolonged culture, the shape of *H. pylori* progressively evolves into a U-shape followed by a
92 spherical form designated coccoid (14, 15). *H. pylori* coccoids are non-culturable bacteria
93 proposed to be dormant forms (15). Recently, dormant non culturable cells were associated
94 wit a deeper state of dormancy when compared to persister cells (16)

95 Coccoids were observed in human gastric biopsies and like spirals adhere to gastric
96 epithelial cells. Despite numerous reports on coccoid forms of *H. pylori*, no cellular effector
97 of this conversion has been reported so far.

98 In type I TAs, the antitoxin is a small regulatory RNA inhibiting the synthesis of the toxin
99 by base pairing the toxin-encoding mRNA (3, 4, 17, 18). Four families (A-B-C-D) of
100 conserved type I TA systems are expressed from the chromosome of *H. pylori*, only the A
101 family was studied as it is highly expressed and conserved among *H. pylori* strains (19, 20).
102 For the A1 TA system, the detailed mechanism by which transcription of the IsoA1 antitoxin
103 RNA impairs AapA1 toxin synthesis by base-pairing with its primary transcript, ensuring
104 both translation inhibition of the AapA1 active message and leading to rapid degradation of
105 the duplex by RNase III has been recently published (20). The *H. pylori* type I toxins are
106 typically small hydrophobic peptides of 30-40 amino acids predicted to form alpha-helices.
107 No clues on the mode of action or the physiological role of these systems have been reported.

108 Here we show that the AapA1 toxin induces a rapid and massive morphological
109 transformation of *H. pylori* from spirals to coccoids by targeting the inner membrane and
110 interfering with cell division, and that oxidative stress triggers imbalanced expression of the
111 TA components in favor of toxin production.

112 **Results**

113 **The AapA1 toxic peptide, expressed by the AapA1/IsoA1 TA system, triggers rapid**
114 **transformation of *H. pylori* into coccoids**

115 Recently, the study of the AapA1/IsoA1 TA system of *H. pylori* (**Fig. 1A**) showed that
116 expression of the AapA1 toxin (a 30 amino acids-long hydrophobic peptide) leads to bacterial
117 growth arrest (20). Given the genetic organization of the type I AapA1/IsoA1 locus in B128
118 strain, we decided to investigate the mechanism underlying the activity of AapA1 by using a
119 strain in which AapA1 is under the control of an inducible promoter. We thus transformed *H.*
120 *pylori* strain B128 deleted of the AapA1/IsoA1 locus with each of the three plasmids
121 constructed by Arnion *et al.* (20) (**Fig. 1A**). The first, pA1-IsoA1, derived of the pILL2157
122 vector (21) contains a functional TA locus in which the AapA1 gene is under the control of an
123 IPTG inducible promoter (20). In plasmid pA1, derived from this first construct, the antitoxin
124 IsoA1 promoter has been inactivated by point mutations that do not interfere with
125 transcription or translation of the AapA1 ORF (20). Derived from this second construct,
126 plasmid pA1* contains an additional mutation that inactivates the start codon of the AapA1
127 peptide (20). Under our experimental conditions, we observed, in agreement with data of (20),
128 that addition of IPTG did not significantly influence the growth rate of strains harboring pA1-
129 IsoA1 or pA1*. In contrast, addition of the inducer causes a rapid and immediate growth
130 arrest of *H. pylori* with pA1 indicating a toxic effect of AapA1 expression (**Fig. 1B**). The
131 growth arrest was accompanied by loss of culturability of more than 10^4-fold 8h after
132 induction.

133 In parallel to growth, we investigated the consequences of AapA1 expression on *H. pylori*
134 morphology. Samples from bacterial cultures with these plasmids were grown in the presence
135 or absence of IPTG, stained with a membrane-specific dye (TMA-DPH) and analyzed by
136 fluorescence microscopy at different time points (**Fig. 1C**). *H. pylori* cells expressing the
137 wild-type AapA1/IsoA1 locus (pA1-IsoA1) or the pA* mutated locus present a classical
138 helical rod shape phenotype upon IPTG exposure (**Fig. 1C**). Under the same conditions, cells

139 carrying the pA1 plasmid, and thus expressing the AapA1 toxin exhibit a rapid and dramatic
140 morphological conversion to spherical cells also known as coccoid forms. Eight hours after
141 IPTG-induction, some bacteria containing pA1-IsoA1 start to convert to coccoids, this is
142 probably due to accumulation of the AapA1 toxin under these conditions. No bacterial lysis
143 was detected even at 24h post-induction. With strains carrying the pA1* plasmid, coccoids
144 were only observed after 48h of culture, similarly to the control wild type strain containing an
145 empty plasmid. These data show for the first time that the AapA1 toxin induces a fast
146 conversion of *H. pylori* cells from spiral-shaped to coccoid forms.
147
148 **Inner membrane targeting by the AapA1 toxin**
149 To investigate the mode of action of the AapA1 toxin, we first analyzed its subcellular
150 localization in *H. pylori* using three reporter strains. Two constructs corresponded to C-
151 terminal fusions of the toxin with a SPA-tag (pA1-SPA) (20) or with GFP (pA1-GFP)
152 expressed from the IPTG-inducible promoter of vector pILL2157 (21) (**Fig. S1**). These
153 plasmids were introduced into *H. pylori* strain B128 deleted of the chromosomal
154 AapA1/IsoA1 module. After IPTG induction none of these fusions affected *H. pylori* growth
155 indicating that a C-terminal fusion prevents the toxicity of the toxin. Attempts to construct N-
156 terminal tagged-AapA1 were unsuccessful. In addition, a B128 derivative expressing a
157 chromosomal AapA1-GFP fusion under control of its native promoter was constructed (**Fig.**
158 **S1**).
159 Cellular fractionation was then performed on the three strains, and the subcellular
160 localization of the fused toxins was analyzed by immunoblotting. **Figure 2A** shows that upon
161 induction by IPTG, the large majority of the AapA1-SPA is present at the inner membrane of
162 *H. pylori* with no peptide detected in the culture medium. Identical results were obtained with
163 the A1-GFP fusion expressed either from the inducible plasmid or the chromosome (**Fig. S2**).
164 Fluorescence microscopy of live bacteria after induction of the AapA1-GFP fusion revealed a

165 weak patchy pattern in the periphery of the cell (**Fig. 2B**), different from a GFP-alone control
166 cell (**Fig. S2**), and compatible with membrane localization. This observation was confirmed
167 by measuring the overlap of the fluorescence intensity profiles of the toxin and TMA-PH
168 measured perpendicular to the length axis of *H. pylori* (**Fig. 2B**).
169 From these results, we conclude that the AapA1 toxin is specifically targeted to the inner
170 membrane of *H. pylori*.
171
172 **AapA1 toxin has a minor impact on *H. pylori* membrane potential and intracellular ATP**
173 **content**
174 Considering the membrane localization of the toxin, we hypothesized that AapA1
175 expression could affect the membrane potential and by consequence the ATP content of the
176 cells. To explore this possibility, *H. pylori* cells harboring pA1-IsoA1, pA1* or pA1 plasmids
177 were taken at different culture time points, stained with a membrane potential sensitive dye
178 (MitoRed CMXROS) and analyzed by microscopy (**Fig. 2C**). Bacteria harboring either an
179 empty plasmid (B128), pA1-IsoA1 or pA1* exhibit a uniform MitoRed CMXROS
180 fluorescence pattern indicative of membrane integrity. For *H. pylori* cells overexpressing
181 AapA1 and converting to coccoids, the fluorescence pattern progressively evolves from
182 uniform to that of discrete foci, suggesting local changes in membrane permeability. No such
183 foci were observed with coccoids from aging WT strain cultures (72h) or with cells treated
184 with 3,5,3',4'-tetrachlorosalicylanilide (TCS), an effective *H. pylori* protonophore (22) that
185 causes an overall MitoRed CMXROS fluorescence loss due to massive dissipation of
186 membrane potential (**Fig. 2C**). Similar results were obtained with the membrane potential
187 sensitive dye DIOC-5, confirming the local effect of AapA1 on *H. pylori* inner membrane
188 (**Fig. S3**). These data indicate that when the AapA1 toxin is expressed in *H. pylori*, the
189 membrane permeability is not globally compromised but probably locally perturbed.

190 Next, the ATP content of *H. pylori* strains carrying either pA1-IsoA1 or pA1 was
191 measured from total metabolites extracted at different culture time points and quantification
192 by a luciferase based-assay (**Fig. 2D**). After 6h of culture, IPTG induction had a minor effect
193 on cellular ATP content of both strains as compared to the drastic consequences observed
194 with the TCS control. Note that at 6h of culture with IPTG, most of the pA1-containing cells
195 have already transformed into coccoids. After 16h, the overall ATP content strongly drops in
196 both strains and IPTG induction causes an additional weak decrease that is poorly changed
197 upon toxin expression by pA1 (**Fig. 2D).**
198 Taken together, these results show that the AapA1 toxin locally perturbs the *H. pylori*
199 membrane potential with no major consequences on the cellular ATP content. We conclude
200 that dissipation of membrane potential is not the major cause of toxin-induced bacterial
201 growth arrest.
202
203 **Ultrastructural analysis of toxin-induced coccoids**
204 For the first time, cryo-electron microscopy (cryo-EM) was used to visualize *H. pylori*
205 coccoids in near-native states. Using this method, we compared exponentially growing
206 bacteria, toxin-induced coccoids and aging coccoids (70h growth) (**Fig. 3**). In exponential
207 phase, the characteristic helicoidal shape of *H. pylori* (strains B128 WT, 4h and pA1-IsoA1,
208 4-8h) was perfectly visible with a uniformly contrasted cytoplasm surrounded by two dense
209 layers of membranes and multiple flagella. The periplasm of variable thickness surrounding
210 the cell is distinguishable as the low-density space between the inner and outer membrane.
211 Strains expressing the toxin (pA1 at 4-8h) have intact flagella and are visible in two major
212 morphotypes. In the first "U" shaped morphology, a round intact outer membrane surrounds a
213 bent intact inner membrane. The second morphotype corresponds to round coccoids of a
214 diameter of approximately 1µm, with visible integrity of both membranes and a central

215 uniformly stained dense cytoplasm. This second morphotype is similar to that of aging
216 coccoids from the WT strain (70h).
217 In conclusion, CryoEM images revealed that the toxin-induced *H. pylori* coccoids have no
218 visible defect in membrane integrity and are ultrastructurally similar to aging coccoid forms.
219

220 **Modification of peptidoglycan composition upon transformation of *H. pylori* into**
221 **coccoids**

222 Our data showed that the AapA1 toxin targets *H. pylori* inner membrane without causing
223 significant membrane potential collapse and without visible loss of integrity. Therefore, we
224 tested whether the toxin-induced cell shape transformation could be associated with
225 modifications in the cell wall and thus in peptidoglycan (PG) composition. PG extracted from
226 B128 WT strain in exponential phase or after 72h growth (aging coccoids) was compared to
227 PG from the pA1 strain induced during 6 and 16h (toxin-induced coccoids). Samples were
228 digested with mutanolysin and subjected to HPLC/MS analyses. The relative abundance of
229 muropeptides in each sample was calculated according to Glauner *et al.* (23) (**Table S1**).
230 When compared to PG of helicoidal *H. pylori*, both "aging" and "toxin-induced" coccoids
231 present similar changes in dipeptide and tripeptide monomers with a stronger effect of toxin-
232 induction at 16h. Coccoids after 16h induction present a 3-fold increase in dipeptide
233 monomers concomitant with tri- and pentapeptide monomers reduction. These data indicate
234 that toxin-induced and aging coccoids undergo similar PG modifications, compatible with a
235 looser PG macromolecule, and suggest that they might be generated by similar mechanisms.
236

237 **Kinetics of the toxin-induced *H. pylori* morphological transformation assessed by live**
238 **cell imaging**

239 To progress in our understanding of the morphological conversion of *H. pylori*, we
240 monitored the entire process of *H. pylori* toxin-induced conversion by live cell time-lapse

241 microscopy under physiological microaerobic conditions in a temperature-controlled chamber.
242 The *H. pylori* B128 strain tested constitutively expressed cytoplasmic GFP, was impaired in
243 motility (by deletion of *flaA* encoding the major flagellar protein) and carried the inducible
244 toxin-expressing plasmid pA1. Individual live *H. pylori* bacteria were monitored in agarose
245 pad by both phase contrast and fluorescence microscopy.

246 First, the general growth features of the strain were established in the absence of the IPTG
247 inducer. Under these conditions, statistics of the data collected showed that the strain has a
248 mean doubling time of 165 min (indicative of optimal growth conditions) with an initial
249 bacterial length of 2.1µm after division and a maximum length prior to division of 3.7µm (**Fig.**
250 **S4**). In a second round of experiments, the inducer was added to the pad and snapshots of the
251 cells were taken at intervals of 10 or 15min during 10h (**Fig. 4**). A total number of 63 cells
252 were analyzed from 4 independent experiments, the data are statistically significant. Two
253 representative movies can also be viewed in **Fig. S5**. Only 14 cells did not show visible cell
254 shape modification while the majority (49 bacteria) went through sequential morphological
255 transformations. We classified the transformation steps into 3 categories: "bending" (U-
256 shaped), "pseudo-coccoid" (quasi-round bacteria) and "donut" (fully developed coccoids) and
257 quantified them (**Fig. 4)**. At 185±8.0 min post-induction, 77% of the cells analyzed had
258 undergone bending. One hundred minutes later, only 12 cells were still at this stage while the
259 others had turned into pseudo-coccoids. Finally, one third of the analyzed cells (21 cells)
260 ended up in the round "donut" shape at 420±25.2 min after toxin-induction.

261 Most interestingly, the length of bacteria just before they entered the first morphological
262 transformation (bending) was 3.48±0.08µm, which precisely corresponds to the maximum
263 length we measured before *H. pylori* division. In addition, we observed many examples of
264 two bacteria that were dividing but not yet separated and from which one out of the two
265 underwent morphological transformation (see movie in **Fig. S5**). This analysis gave us a
266 dynamic picture of the morphological transformation of *H. pylori.* Importantly, this analysis

267 strongly suggests that the morphological transformation is consecutive to a toxin-induced
268 perturbation of cell division, through a mechanism that is still to be defined.
269
270 **Toxin-antitoxin imbalanced expression upon oxidative stress**
271 We then searched what physiological signal could trigger the induction of the AapA1 toxin
272 expression in *H. pylori*. First, the respective activities of individual *aapA1* and *IsoA1*
273 promoters were measured with chromosomally expressed transcriptional *lacZ* fusions (**Fig.**
274 **S1**). Under normal growth conditions, ß-galactosidase activities indicated that the antitoxin
275 promoter has a 10-fold stronger activity than the toxin promoter (**Fig. 5A**). This result is
276 consistent with type I TA features where the antitoxin RNA is strongly expressed (but highly
277 labile) compared to the more stable toxin transcript that is expressed at a lower level (7, 8, 18).
278 The *lacZ* fusions were then used to follow the activity of the two promoters during *H. pylori*
279 growth and to search for conditions relevant to *H. pylori* life-style that could lead to
280 imbalanced expression of the two promoters. Only a slight increase in activity of both
281 promoters was observed over time of growth (**Fig. 5A**). No significant differential expression
282 of the promoters was observed upon acid, antibiotic stress or during exposure to high nickel
283 concentrations (**Fig. S6**). In contrast, oxidative stress induced by hydrogen peroxide (H_2O_2)
284 resulted in a strong specific decrease in the *IsoA1* promoter activity while, at the same
285 concentration, the toxin promoter activity was marginally reduced (**Fig. 5B**). Exposure to
286 paraquat, another oxidative stress agent, resulted in a comparable strong decrease of both
287 promoters. The expression patterns and stability of the *aapA1* and *IsoA1* transcripts were then
288 analyzed by Northern Blot with total RNA extracted at different time points after rifampicin
289 addition. As shown in **Fig. 5C** and **Fig. S7**, the *aapA1* transcript was detected as a 175
290 nucleotide-long band with an estimated half-life of approx. 120min. In contrast, the 75 nt
291 *IsoA1* full length transcript declines much faster, with an estimated 25min half-life, and the
292 production of an approx. 50 nt short processed form. Upon hydrogen peroxide exposure, the

293 half-life of the AapA1 transcript was not significantly modified while we observed a more
294 rapid depletion of the full-length *IsoA1* transcript with an almost immediate accumulation of
295 the processed form (**Fig. 5C**). From three independent experiments, we quantified the relative
296 amounts of the transcripts under normal growth conditions versus H_2O_2 exposure during 120
297 min after rifampicin addition (**Fig. 5D**). No significant change was observed for the *aapA1*
298 transcript while H_2O_2 exposure resulted in a diminished half life of the *IsoA1* full length
299 transcript and in an imbalanced ratio of *IsoA1* in favor of its processed form (**Fig. 5D**). Taken
300 together, these results show that H_2O_2 causes both diminished *IsoA1* transcription and
301 increased degradation of *IsoA1* full-length transcript. These observations suggest that, by
302 decreasing the amounts of antitoxin transcript, exposure to oxidative stress favors translation
303 of the AapA1 mRNA and thus toxin production.
304
305 **Oxidative stress induction of coccoids: are class A Type I TA the only effectors ?**
306 Since we established that oxidative stress results in imbalanced expression in favor of the
307 expression AapA1 toxin, we examined the consequences of exposure to this condition on *H.*
308 *pylori* morphology and viability. Upon H_2O_2 oxidative stress, we observed a rapid
309 transformation into coccoids (approx. 6h) in strain B128. This strain contains six class A type
310 I TA systems, the A2 locus being inactive (**Fig. S8**). To assess their role, we constructed
311 mutants carrying deletions of each of its active AapA/IsoA TA loci, Δ*A1*, Δ*A3*, Δ*A4*
312 (including deletion of both *A4-1* and *A4-2* tandem systems), Δ*A5*, Δ*A6* or of the five loci
313 collectively (Δ*5*) using a non-marked deletion strategy (24). Under normal conditions, the
314 growth rate, culturability and kinetics of occurrence of coccoids of the different mutants was
315 similar to that of the parental strain (**Fig. S9**). Upon H_2O_2 oxidative stress, the Δ5 mutant
316 strain displayed similar kinetics of conversion to coccoids when compared to the parental
317 strain.

318 This shows that oxidative stress is triggering transformation into coccoid but that the type I
319 toxins are not the only effectors. TA systems have been shown to play a role in persister cell
320 formation under stress conditions (7, 8). Therefore, the number of persisters after exposure to
321 hydrogen peroxide was measured for the ΔA1 and Δ5 mutants and compared to the parental
322 strain (**Fig. S9**). No significant difference was observed, suggesting that, upon hydrogen
323 peroxide stress, the class A TA systems are not promoting viable persisters in *H. pylori*.
324

325 **Discussion**

326 Here we established that the expression of a small toxin from a toxin-antitoxin system
327 triggers a massive and rapid morphological transformation of the spiral-shaped *H. pylori*
328 bacterium into round coccoid cells. Transformation of spirals into coccoids has been observed
329 after extended *H. pylori* growth (>70h, aging coccoids) or upon stress conditions (14) but the
330 process itself was poorly characterized. The toxin (AapA1) is a small hydrophobic peptide of
331 a type I TA system that we showed here to target *H. pylori* inner membrane without being
332 secreted. Toxins of type I TA system from other organisms such as *Escherichia coli*, *Bacillus*
333 *subtilis* or *Staphylococcus aureus* have been shown to localize to the inner membrane but
334 there are no reports on induction of major cell shape modifications (8, 25-27). The *E. coli*
335 TisB (28) and the *S. aureus* PepA1 (29) toxins act by creating membrane pores (similar to
336 phage holins) thereby disrupting the membrane potential, drastically impairing ATP synthesis
337 and depending on the toxin concentration, either leading to the formation of persisters or to
338 cell death (8, 27). One notable exception is the BsrG/SR4 Type I TA system of *B. subtilis*
339 (26). The BsrG toxin was found to target the membrane without causing destruction or
340 affecting the Proton Motive Force but it rather directly interferes with the cell envelope
341 biosynthesis, indirectly delocalizes the cell-wall synthesis machinery and ultimately triggers
342 bacterial autolysis (26). There are now two examples of type I TA hydrophobic toxins (BsrG
343 and AapA1 reported here) that do not act by permeabilizing the membrane and probably
344 reflect a novel mode of action for small peptidic toxins.

345 Using for the first time cryo-EM, we observed that toxin-induced *H. pylori* coccoids
346 present neither visible membrane disruption nor pores even 8h post toxin induction and are
347 ultrastructurally comparable to 70h-old aging coccoids. The membrane potential of coccoids
348 was not dissipated despite the fact that the toxin induces local perturbation of the membrane.
349 This is in contrast with a previous study that reported a total loss of membrane potential in *H.*
350 *pylori* aging coccoids, associated with a complete loss of membrane integrity (30). Unlike the

351 effects of the TisB toxin in *E. coli* (28), we found that the ATP content in our *H. pylori* toxin-
352 induced coccoids is marginally affected and drops only after prolonged culture, as it is the
353 case for spiral-shaped cells (31).

354 Toxins expressed by TA systems cause growth arrest by interfering with conserved vital
355 cellular processes such as translation, division or peptidoglycan (PG) synthesis (8, 27). In
356 bacteria, PG cell-wall dictates cell shape. We found that coccoid transformation was
357 accompanied by changes in PG composition. Indeed, when compared to spirals, coccoids
358 have a three-fold increase in dipeptide monomers concomitant with a tri- and pentapeptide
359 monomers reduction. These changes are comparable to those previously reported for "aging"
360 *H. pylori* coccoids (32) and were confirmed here. Our results point to a reduction in the
361 potential for generating new cross-bridges in the PG; this is compatible with a looser PG
362 macromolecule and could explain the morphological transition to coccoids. The PG
363 metabolism has been extensively studied in *H. pylori* (33). The modifications we observed in
364 coccoids suggest activation of at least three sequential *H. pylori* PG hydrolase activities. A
365 D,D-carboxypeptidase that transforms pentapeptides into tetrapeptides; HdpA/Csd3 is the
366 only reported such enzyme (34). A L,D-carboxypeptidase that transforms tretapeptides into
367 tripeptides carried out by Csd6, a member of the L,D-transpeptidases (33). Finally, a (g)-
368 glutamyl-diaminopimelate carboxypeptidase generating dipeptides from tripeptides carried
369 out by Cds4, a member of the M14-zinc metallopeptidases (33). We previously showed that
370 these three PG modifications are blocked in a mutant deficient in AmiA, a putative *H. pylori*
371 amidase and that an *amiA* mutant fails to transform into coccoids (35). Therefore, we propose
372 that AmiA could be a central hub for the functionality of a PG hydrolase complex including
373 AmiA, HdpA, Csd4 and Csd6. In this case, the AapA1 toxin would interfere with the function
374 of this complex by causing abnormal activation of their enzymatic activities.

375 Life imaging analysis of the toxin-induced conversion of *H. pylori* spirals into coccoids
376 suggested that the AapA1 toxin interferes with cell division. This is also consistent with a

377 central role of AmiA in the conversion, indeed this enzyme was shown to be essential for the
378 separation of daughter cells (35). In *E. coli*, the CbtA toxin of a type IV TA system was found
379 to inhibit cell division and cell elongation via direct and independent interactions with FtsZ
380 and MreB (36). More work is needed to identify the molecular target(s) of the AapA1 toxin.

381 Under normal conditions, as for all TA systems, the *IsoA1* antitoxin potently inhibits the
382 AapA1 toxin, by preventing its expression through a multilayered mechanism (20). We
383 searched for physiological conditions that could result in toxin expression. We found that
384 oxidative stress, generated by H_2O_2, causes a rapid and specific decline in the levels of IsoA1
385 antitoxin full-length transcript by reducing both its promoter activity and enhancing its
386 degradation through a mechanism that remains to be precisely defined. Imbalanced expression
387 of the AapA1/IsoA1 system in favor of the toxin mRNA should lead to toxin expression.
388 Accordingly, we observed that H_2O_2 causes a rapid conversion of *H. pylori* into coccoids
389 resembling those induced by the AapA1 toxin. Prolonged exposure to aerobic conditions was
390 previously reported to lead to the coccoid formation, however, in that case these cells lost
391 their membrane integrity (37). Regulation of type I TA systems in response to stress had been
392 observed in other species. For the *bsrE*/SR5 type I system of *B. subtilis*, the SR5 antitoxin is
393 affected by pH, anoxia and iron limitation while the BsrE toxin is sensitive to temperature
394 shock and alkaline stress (38). In *S. aureus*, the SprA1/SprA1$_{AS}$ system is induced in response
395 to acidic or oxidative stresses (29). In *E. coli*, several type I toxins are induced by the SOS
396 response (7), a system that does not exist in *H. pylori*.

397 The biological function of *H. pylori* coccoids is still a matter of debate. Coccoids are
398 observed in prolonged *in vitro* cultures and induced by stress conditions, mostly aerobic,
399 anaerobic culture or exposure to antibiotic or oxidative stress. However, these reports are
400 difficult to compare since no standard procedure was used and analysis was most of the time
401 performed after more than a week stress exposure (14, 30, 39). *H. pylori* coccoids are non-
402 culturable cells under standard laboratory growth conditions. Our analysis of both toxin-

403 induced and 70h aging coccoids are in favor of their viability despite their "unculturability".
404 We argue that contradictory conclusions on viability refer to "damaged" or so-called
405 "fragmented" coccoid forms corresponding to membrane-less bacteria in prolonged *H. pylori*
406 cultures (30). In favor of coccoid viability are previous reports showing that coccoids express
407 virulence factors (14) and are capable, like spirals, of binding to host cells and inducing
408 cellular changes (40). *H. pylori* coccoids were also visualized in human gastric biopsies (41),
409 probably as part of biofilms (39). In mice, coccoids induce gastritis (42) and can revert to
410 colonizing spiral bacteria (43). Taken together, these observations suggest that coccoids are
411 "dormant" viable forms of *H. pylori* that recover during host infection and might play a role
412 in transmission or in treatment failure. In agreement with this view, Chaput *et al.* (35) showed
413 that coccoids present decreased activation of NF-kB and might allow the bacterium to escape
414 the host immune response.

415 We showed that *H. pylori* coccoids are induced by a class A type I TA toxin and by
416 oxidative stress probably through the imbalanced expression of TA systems. During infection,
417 *H. pylori* is indeed exposed to harsh oxidative stress as a consequence of the chronic
418 inflammation it generates (44). Deletion of the five "class A" Type I TA clusters of *H. pylori*
419 did not preclude the oxidative stress induction of coccoids nor did it change the number of
420 persister cells. We concluded that these toxins are probably not the only triggers of coccoid
421 transformation and suggest that the two other classes of chromosomally-encoded type I TA
422 systems (B and C representing 9 systems) might also be important.

423 Dormant/persister bacteria present enhanced tolerance to antibiotics and it has been shown
424 that they can be induced by TA systems (7, 8), although other mechanisms resulting in
425 lowered ATP content are also associated with their occurrence (11). We hypothesize that TA-
426 induced *H. pylori* coccoids are dormant bacteria and, as previously proposed, that non-
427 culturable cells and "classical" dormant bacteria/persisters are part of a shared "dormancy

428 continuum" (45). In our model, this continuum would depend on the intracellular toxin
429 concentration as already suggested (46).

430 Stress-induced morphological transformation of bacteria into non-culturable coccoid-like
431 cells has been reported in at least 85 bacterial species among which important bacterial
432 pathogens such as *Campylobacter jejuni, Vibrio cholerae* or *Salmonella typhimurium* (16).
433 For these organisms, the inducing trigger and function remains to be characterized. We
434 postulate that these forms are dormant bacteria and that our findings on *H. pylori* might be
435 more generally relevant and play important roles in recurrent and persistent bacterial
436 infections.

437

438

439 **Figure legends**

440 **Figure 1: Expression of the AapA1 toxin from the AapA1/IsoA1 TA system induces**
441 **growth arrest and transformation of *H. pylori* strain B128 into coccoids.**

442 **A)** Genetic organization of AapA1/IsoA1 locus in *H. pylori* B128 strain with the AapA1
443 transcript encoding the toxin and the *IsoA1* antitoxin RNA. Below is the representation of the
444 inserts of the three plasmids constructed by Arnion *et al* (20) and used in this study, each
445 derived from the pILL2157 *E. coli/H. pylori* vector (21). These inserts are expressed under
446 the control of an IPTG inducible promoter. Plasmid pA1-IsoA1 expresses both the toxin and
447 the first 30 nucleotides of the *IsoA1* RNA antitoxin. In pA1, the promoter region of IsoA1
448 was mutated without affecting the amino acid sequence of AapA1. Plasmid pA1* was derived
449 from pA1 and contained an additional mutation inactivating the start codon of AapA1.

450 **B) Expression of the AapA1 toxin causes rapid growth arrest of *H. pylori* strain B128.**
451 Growth kinetics of *H. pylori* B128 strains carrying each of the three plasmids illustrated in
452 panel A, grown in the absence (black symbols) or in the presence of 1mM IPTG (empty
453 symbols) that was added at the time indicated by an arrow (16h).

454 **C) Expression of the AapA1 toxin induces transformation of *H. pylori* into coccoids.**
455 Microscopy analysis of the *H. pylori* B128 strains carrying each of the three plasmids after
456 growth in the absence of IPTG or at 4 and 8h following IPTG addition. *H. pylori* membranes
457 were stained with the lipophilic dye TMA-DPH. Phase-contrast and fluorescence images are
458 respectively represented on the upper and bottom panel. The scale bar corresponds to 1μm.

459

460 **Figure 2: AapA1 toxin targets *H. pylori* inner membrane, weakly disturbs the bacterial**
461 **membrane potential and poorly affects intracellular ATP content.**

462 **A) AapA1 toxin localizes to the *H. pylori* inner membrane.** Western blot analysis of total
463 extracts (T), soluble extracts (SE), inner membrane (IM) and outer membrane (OM) fractions

464 prepared from *H. pylori* B128 strain expressing either a SPA tagged-AapA1 toxin (pA1-SPA)
465 under control of an IPTG-inducible promoter or carrying plasmid pA1* as a negative control.
466 The fractionation procedure was validated with antibodies against the following control
467 proteins, PBP2 for the inner membrane, AlpA for the outer membrane and NikR for the
468 cytoplasm. In **Fig. S2**, we show that a A1-GFP fusion expressed either from the chromosome
469 of B128 or from a plasmid also localizes at the inner membrane.

470 **B) In live cells, AapA1-GFP localizes as discrete foci around the *H. pylori* membrane.**
471 Strain B128 expressing the AapA1-GPF fusion protein was analyzed on agarose pads by
472 fluorescence microscopy 6h after IPTG-induction. Membranes were stained with TMA-DPH
473 lipophilic dye. The membrane association of AapA1-GPF was quantified by measuring the
474 fluorescence intensity profile perpendicular to the length axis of *H. pylori*. The graph shows
475 the average fluorescence intensity profiles with standard deviation (n=25). The fluorescence
476 maxima separated by 0.5 μm, correlate with the *H. pylori* cell width.

477 **C) Analysis of the effect of the AapA1 toxin on *H. pylori* membrane potential.**
478 MitoRed CMXROS, a membrane potential reactive dye was used to analyze live *H. pylori*
479 B128 strains expressing each of the three plasmids illustrated in **Fig. 1**. Cells were grown in
480 presence or absence of 1mM IPTG and analyzed on agarose pads at 0, 4, 8 and 24 h after
481 IPTG addition. While uniformly stained by the MitoRed CMXROS in the absence of IPTG,
482 cells expressing the toxin (pA1) present discrete foci of stronger fluorescence suggesting a
483 local disturbance of the membrane potential. For comparison, a 72h-old culture of B128 WT
484 strain forming "aging" coccoids was also analyzed. As a positive control of membrane
485 potential loss, 4h-old B128 WT cells were analyzed after treatment or not with TCS (3,3',4',5-
486 Tetrachlorosalicylanilide) an *H. pylori* active protonophore. Bar scale represents 1μm.

487 **D) Measurement of intracellular ATP content.**
488 Intracellular ATP was extracted from B128 strains harboring pA1-IsoA1 or pA1 after 6 or
489 16h growth in the presence or absence of IPTG. B128 WT strain treated with 500μM of TCS

490 protonophore was used as a positive control. ATP concentrations were determined using a
491 luciferase-based assay (BacTiter-Glo™, Promega). Results from 3 independent experiments
492 performed in triplicates are shown. Error bars represent the standard deviation, with * and **
493 indicating that the mean value is significantly different, * corresponds to $P < 0.05$, ** to $P <$
494 0.01, *** to $P < 0.001$ and NS corresponds to non-significant, ($P > 0.05$).
495
496 **Figure 3: Ultrastructural analysis of toxin-induced coccoids and "aging" coccoids by**
497 **cryo-electron microscopy.**
498 Cryo-electron microscopy was used to compare "aging" coccoids (70 h-old cultures) and
499 exponentially growing B128 strains carrying plasmid pA1-IsoA1 or pA1 grown for 4 or 8h in
500 the presence of IPTG. Expression of the toxin results in the formation of U-shaped bacteria at
501 4h and round coccoids cells at 8h with visible intact bacterial cell envelop similar to the aging
502 coccoids. Scale bar represents 1μm.
503
504 **Figure 4: Time-lapse microscopy of *H. pylori* conversion to coccoid upon toxin**
505 **expression.**
506 Live cell time lapse microscopy was used to record, during 10 hours, the morphological
507 modifications of individual *H. pylori* B128 strain cells after IPTG-induction of the AapA1
508 toxin. Phase-contrast and fluorescence images of one example of these kinetics are presented.
509 Scale bar represents 2μm. Three major phenotypes were observed; "bending", "pseudo-
510 coccoids" and "donut". Statistics (median and mean ± SEM) on the total number of analyzed
511 cells and the precise timing to reach the phenotypes are presented. SEM corresponds to
512 standard error of the mean. Representative movies of the transformation can be seen in **Fig.**
513 **S5**.
514

515 **Figure 5: Oxidative stress generated by hydrogen peroxide results in decreased antitoxin**
516 **promoter activity and promotes *IsoA1* transcript processing.**
517 **A) Activity of the AapA1 and IsoA1 promoters as a function of growth.**
518 β-galactosidase activities (expressed in Miller units) measured with *H. pylori* B128 strain
519 carrying chromosomal P*aapA1-lacZ* and P*IsoA1-lacZ* fusions after 6, 24 and 48h growth.
520 Results from 3 independent experiments performed in duplicates are shown. Error bars
521 represent the standard deviation, with * ($P < 0.05$) and ** ($P < 0.01$) indicating that the mean
522 values are significantly different and NS indicating that they are not significantly different (P
523 >0.05). The activity of the toxin fusion (*aapA1-lacZ*) is about ten times that of the antitoxin
524 fusion (*IsoA1-lacZ*) and the activity of both promoters slightly increases as a function of
525 growth.
526 **B) Oxidative stress generated by H_2O_2 decreases antitoxin promoter activity.**
527 β-galactosidase activities expressed by P*aapA1-lacZ* and P*IsoA1-lacZ* fusions were measured
528 after 6h treatment with oxidative stress generators, paraquat (5, 50 and 500 μM) and H_2O_2
529 (0.03 and 0.3%). β-galactosidase activities are presented as ratio (expressed in %) of activities
530 measured with stress versus activities of untreated samples. Hydrogen peroxide strongly
531 decreases the expression of the P*IsoA1-lacZ* fusion. Results from 3 independent experiments
532 performed in duplicates are shown. Error bars represent the standard deviation, with * ($P <$
533 0.05), ** ($P < 0.01$), *** ($P <0.001$) indicating that the mean values are significantly different
534 and NS that they are not significantly different ($P >0.05$).
535 **C) Determination of AapA1 mRNA and IsoA1 RNA half-lives in *H. pylori* strain B128**
536 **under normal conditions and upon hydrogen peroxide exposure.**
537 Northern blots of total RNA from B128 WT strain grown under normal conditions or exposed
538 to 1% hydrogen peroxide, extracted at the indicated times after addition of 80 μg/ml
539 rifampicin. Five μg of RNA were loaded in each lane and the membranes were probed with

540 [γ-^{32}P] ATP-labeled oligonucleotides specific to the following RNAs, *aapA1*, *IsoA1* and 5S
541 rRNA as a loading control. In the presence of H_2O_2, the half-live of *IsoA1* transcript is
542 diminished in favor of the processed *IsoA1* form.

543 **D) Hydrogen peroxide promotes *IsoA1* transcript processing.**

544 Graphic representation of the effects of hydrogen peroxide exposure on the amounts of *aapA*
545 and *IsoA1* transcripts as well as on *IsoA1* processing during 120 min after rifampicin addition.
546 The relative amounts of *aapA1* (upper graph) and full length (FL) *IsoA1* (middle graph)
547 RNAs versus 5S rRNA are shown. The lower graph presents the relative amounts of the two
548 forms of *IsoA1*, full length (FL) versus the processed form. The results of 3 independent
549 experiments are shown, error bars represent the standard deviation analyzed by two-way
550 ANOVA multiple comparisons.

551

552

553 **Acknowledgments**

554 This work was funded by the Agence National de la Recherche (ANR 09 BLAN 0287 01 and
555 ANR 12 BSV5-0025-02), the Laboratoire d'Excellence IBEID (Integrative Biology of
556 Emerging Infectious Diseases) Grant ANR-10-LABX-62-IBEID from the French
557 government's Investissement d'Avenir program and the Pasteur-Weizmann Consortium of
558 "The Roles of Noncoding RNAs in Regulation of Microbial Life Styles and Virulence". LEM
559 was funded by a Roux fellowship of the Institut Pasteur and by a Carnot MI fellowship. AR
560 was supported by post-doctoral fellowship from the Labex IBEID (10-LABX-62-IBEID). We
561 also thank Janssen for financial support. We are grateful to F. Darfeuille and H. Arnion for
562 the gift of plasmids and to W. Fischer for the gift of anti-AlpA antibodies. We also appreciate
563 the expertise and help of A. Chery-Faleme, M. Fromont-Racine and A. Jacquier with
564 Northern blotting and of R. Wheeler for peptidoglycan extraction. We thank M. Denic, S.
565 Kumar and A. Tejada-Arranz for comments on the manuscript and J. Berry for discussions.
566 Finally, we thank M. Nilges and the Equipex CACSICE for providing the Falcon II direct
567 detector.

568

569 **Material and Methods**

570

571 ***Bacterial strains and growth conditions***

572 The *H. pylori* strains used in this study (Suppl **Table S2**) were all derived of strain B128
573 (47) (48). Plasmids (suppl **Table S3**) used to create or complement *H. pylori* mutants were
574 constructed and amplified using *E. coli* One-Shot TOP10 or DH5α strains (Thermofisher). *H.*
575 *pylori* strains were grown on Blood Agar Base 2 (Oxoid) plates supplemented with 10%
576 defibrinated horse blood and with the following antibiotics-antifungal cocktail: amphotericin
577 B 2.5 $\mu g.ml^{-1}$, polymyxin B 0.31 $\mu g.ml^{-1}$, trimethoprim 6.25 $\mu g.ml^{-1}$ and vancomycin 12.5
578 $\mu g.ml^{-1}$. Selection of *H. pylori* mutants was performed using kanamycin 20 $\mu g.ml^{-1}$,
579 Streptomycin 10$\mu g.ml^{-1}$, Apramycin 10$\mu g.ml^{-1}$ or chloramphenicol 8 $\mu g.ml^{-1}$. For liquid
580 cultures, we used Brain Heart Infusion (BHI) broth (Oxoïd) supplemented with 10% Fetal
581 Calf Serum (FCS) (Eurobio), the antibiotics-antifungal cocktail and the selective antibiotic
582 when necessary. *H. pylori* cells were grown at 37°C under microaerophilic atmosphere
583 conditions (6% O_2, 10% CO_2, 84% N_2) using an Anoxomat (MART Microbiology)
584 atmosphere generator. When indicated, 1mM of isopropyl ß-D-1-thiogalactopyranoside
585 (IPTG, EuroMedex) was added to agarose pads or culture media.

586

587 ***Molecular techniques***

588 Molecular biology experiments were performed according to standard procedures and the
589 supplier (Fermentas) recommendations. NucleoBond Xtra Midi Kit (Macherey-Nagel) and
590 QIAamp DNA Mini Kit (Qiagen) were used for plasmid preparations and *H. pylori* genomic
591 DNA extractions, respectively. PCR were performed either with Taq Core DNA polymerase
592 (MP Biomedicals), or with Phusion Hot Start DNA polymerase (Finnzymes) when the
593 product required high fidelity polymerase. The pGEM-T easy vector systems (Promega) was

594 used to construct in *E. coli*, the suicide plasmids that served for markerless deletions of TA
595 systems in *H. pylori*.
596
597 ***Construction of H. pylori strains carrying mutation or plasmids***
598 Mutations of *H. pylori* were introduced into strain B128 either WT or a streptomycin
599 resistant variant B128 *rpsL1* for markerless mutagenesis (24, 49). Chromosomal deletions of
600 the *AapA1/*IsoA1 locus, of the *flaA* gene, or of the different class A TA loci were performed
601 either by insertion of a selectable antibiotic resistance marker to disrupt or replace the gene of
602 interest or when necessary, by the markerless counter-selected mutagenesis strategy (24, 49).
603 Plasmids were derived from the pILL2157 *E. coli/H. pylori* shuttle vector that contains an
604 IPTG-inducible promoter (21). Deletions were introduced by allelic exchange using suicide
605 plasmids (see suppl **Table S3**) or PCR fragments. Introduction of plasmids and construction
606 of *H. pylori* mutants were obtained by natural transformation and selection with the
607 corresponding antibiotic as described previously (24). PCR and sequencing of the regions of
608 interest were used to validate the introduction of plasmids, deletion of genes of interest and
609 correct insertion of fusions. Primers used for these constructs or their validation are listed in
610 Suppl **Table S4.**
611
612 **Confocal Fluorescence Microscopy**
613 Fluorescence microscopy was performed with an Axio Observer microscope (Zeiss)
614 equipped with an Axiocam camera under an X100 magnification. Acquisition images was
615 performed using the axiovision software. Images were cropped and adjusted using ImageJ
616 1.47v software. *H. pylori* B128 strains were grown in BHI medium with chloramphenicol (8
617 µg/ml) to maintain the plasmids. IPTG was added to the culture and samples were taken at
618 different time-points, concentrated by 2 min centrifugation at 3000 x g and washed twice with
619 PBS buffer. Cells were immobilized using 2% (wt/vol) agarose pads containing PBS before

620 being imaged. In **Fig. 1C**, cell membranes were stained with 0.01 mM TMA-DPH (1-(4-
621 trimethylammoniumphenyl)-6-phenyl-1,3,5-hexatriene p-toluenesulfonate, Euromedex).
622 Membrane potential was revealed with 25nM MitoTracker®Red CMXROS (Invitrogen) in
623 **Fig. 2C** and with 1µM DIOC-5 (3) (3,3-Dipentyloxacarbocyanine iodide, Interchim) in **Fig.**
624 **S3**. For the membrane potential analysis, the negative control was obtained by treatment with
625 the protonophore 500µM TCS (3,3',4',5-Tetrachlorosalicylanilide; Fisher scientific).
626
627 **Fractionation and Immunoblotting**
628 The protocol of *H. pylori* fractionation was adapted from (50). *H. pylori* strains were
629 grown in the absence or presence of 1mM IPTG. When cultures reached OD_{600} 0.8, cells were
630 harvested by centrifugation, washed twice in phosphate-buffered saline medium (PBS) prior
631 to their disruption by sonication in Buffer 1, 10mM Tris-HCl, pH7.5 containing 5mM ß-
632 mercaptoethanol and proteases inhibitors (cOmplete™, EDTA-free Protease Inhibitor Cocktail,
633 Roche). Cell debris were removed by centrifugation (10 min, 16,000 x *g*, 4°C) and
634 supernatants containing the soluble extract and membrane fractions were collected as total
635 extracts. Samples of total extracts were frozen and the remaining supernatants were subjected
636 to ultracentrifugation (125,000 x *g*, 45 min, 4°C). Samples from the supernatant containing
637 the cytoplasm and periplasm were collected and frozen while pellets containing total
638 membranes were resuspended in buffer 1 supplemented with 1% N-lauroylsarcosine (Buffer
639 2) prior to be ultracentrifuged (125,000 x *g*, 45 min, 4°C). Samples of inner membrane
640 fractions from supernatants were frozen. Outer membrane pellets were washed twice in buffer
641 2 to avoid inner membrane fractions contamination prior to freezing. In each fraction, protein
642 amounts were calibrated using the Bradford DC Protein Assay (Biorad) with bovine serum
643 albumin (BSA) as a standard. For each cellular compartment, equal protein amounts were
644 loaded and separated on a 4-20% Mini-Protean TGX precast protein gel (BioRad) and
645 subsequently electrotransferred on a polyvinylidene difluoride (PVDF) membrane (Biorad).

646 The *H. pylori* proteins PPB2, AlpA and NikR as well as the fusion protein A1-SPA or A1-
647 GFP were detected with rabbit polyclonal antibodies α-PBP2 (51), α-AlpA (50), α-NikR
648 (52); with mouse monoclonal anti-FLAG M2 antibody (Sigma-Aldrich) or with goat anti-
649 GFP-HRP antibody (Abcam) at the respective dilutions of 1:2,000, 1:1,000, 1:100 and
650 1:1,000 or 1:5,000. Goat anti-rabbit IgG-HRP (Santa Cruz) and ECL anti-mouse IgG
651 Horseradish Peroxydase (Amersham) were used as secondary antibodies and the detection
652 was achieved with the ECL reagent (Pierce).

653

654 **ATP extraction and assay**

655 Exponentially growing *H. pylori* cells (6h of culture OD_{600nm} 0.35) and stationary growing
656 cells (16h, OD_{600nm} 3) were harvested by centrifugation at room temperature for 4 min at
657 5000*g*. Metabolites from the resulting cell pellets were extracted immediately using 300µL of
658 a solvent mixture of Acetonitrile/Methanol/H_2O (40/40/20) for 15min at 4°C and 10min at
659 95°C. Mixtures were subsequently spun in a microfuge for 5 min at maximum speed and 4°C
660 to separate insoluble materials from the extracted metabolites. The resulting pellets were then
661 re-extracted twice with 200 µL of solvent at 4°C. The supernatants were pooled to yield 700
662 µL of final extract. Metabolites were lyophilized and subsequently diluted in water for ATP
663 assays. ATP content was determined by a luciferase based ATP bioluminescence assay kit
664 (BacTiter-Glo™ Microbial cell viability assay, Promega). Luminescence values were
665 determined using a 10 sec RLU signal integration time and measured using a Centro XS^3
666 LB960 Luminometer (Berthold Technologies). ATP concentrations were calculated based on
667 values determined using serial dilutions of known amounts of ATP and expressed as a
668 function of the OD_{600nm} of the corresponding culture.

669

670 **Cryo-electron microscopy**

671 Four µL of *H. pylori* bacteria were spotted on glow-discharged lacey grids (S166-3, EMS) or
672 Quantifoil R2/2 (Quantifoil, Germany). The samples were cryo-fixed by plunge freezing at -
673 180°C in liquid ethane using a Leica EMGP (Leica, Austria). Grids were observed at 200kV
674 with a Tecnai F20 (Thermo Fisher Scientific). Images were acquired under low-dose
675 conditions using the software EPU (Thermo Fisher Scientific) and a direct detector Falcon II
676 (Thermo Fisher Scientific).
677
678 **Time-lapse microscopy**
679 Confocal analysis of live cells was performed as previously described (53). Twenty µL of
680 exponentially grown bacteria (10^5 cells) suspended in BHI with or without 1mM IPTG were
681 deposited on 35mm glass bottom Petri dishes. The suspension was covered with BHI medium
682 in 1.5% low melting agarose supplemented with Chloramphenicol (8µg/µl) with or without
683 IPTG (1mM). Live-cell imaging was performed with a Nikon A1R confocal laser scanning
684 microscope system attached to an inverted ECLIPSE Ti (Nikon Corp., Tokyo, Japan) and
685 equipped with an environmental chamber allowing the control of temperature (37°C),
686 humidity (90%) and gas mixture (10% CO_2, 3% O_2). GFP fluorescence images were captured
687 through a Plan APO 60X objective (NA: 1.40) by using optimal spatial resolution settings.
688 The cytoplasm compartment volume was defined by using GFP staining (excitation with 488
689 nm laser, emission collected with an 500/50 nm filter set). Image captions were performed
690 every 10min during 10h. Statistics were performed on a total of 63 cells from 4 independent
691 experiments. Image treatment and analysis were performed using NIS elements (Nikon Corp.,
692 Tokyo, Japan) and ImageJ software.
693
694 **ß-galactosidase activity assays**
695 B128Δ*AapA1-IsoA1::PaapA1-lacZ-Kan* and B128Δ*AapA1-IsoA1::PIsoA1-lacZ-Kan*
696 strains were grown to OD_{600nm} 0.3 in BHI liquid medium, then divided into two samples, one

697 of them being submitted to stress conditions during 6h with 5, 50 and 500 µM paraquat
698 (Sigma), 0.03 and 0.3% hydrogen peroxide (Sigma), 20 and 200 mM $NiCl_2$ (Sigma), 0.1 and
699 1 mg/mL tetracycline, or 0.05 and 0.5 mg/ml rifampicin. Then 0.5ml samples were taken,
700 washed twice with 1X PBS (Phosphate Buffered Saline) and further permeabilized with
701 100µL Chloroform and 50µl SDS 0.1% in Z buffer containing 70mM $Na_2HPO_4.12H_2O$,
702 30mM NaH_2PO_4. H_2O, 1mM $MgSO_4$ and 0.2mM $MnSO_4$ (54). Samples were briefly vortexed
703 and incubated at 28°C for 2 min. The ß-galactosidase assay was started by adding 0.5mL
704 ONPG (ThermoFischer) at 4mg/ml and stopped by the addition of 0.5mL 1M Na_2CO_3 when
705 sufficient yellow color was reached. The ß-galactosidase activity is expressed in Miller units
706 (54) and represented in **Fig. 5** and **S6** as percentage of activities relative to the control activity
707 with the corresponding strains not exposed to stress and was calculated from 3 independent
708 experiments performed in duplicates.
709
710 **Total RNA extraction and Northern blotting**
711 Total RNAs were extracted from 10 mL *H. pylori* cultures (OD_{600} 0.5 -0.9) exposed or not to
712 1% H_2O_2 using the NucleoSpin miRNA kit (Macherey Nagel) at different time points after
713 80 µg/mL rifampicin addition (to stop transcription). For Northern blotting, 5 µg of total RNA
714 were separated on 10% Mini protean TBE Urea gel (Biorad) and transferred to Hybond N+
715 (Amersham Biosciences) membrane susing a Trans-Blot Turbo system (Biorad). A DNA
716 marker was used for size estimation.
717 Transferred RNA was fixed to the membrane by UV irradiation for 2 min. The membrane
718 was blocked for 45 min at 42°C with ULTRAhyb Hybridization Buffer (Ambion), then 20 µl
719 of 5'-labeled ($\gamma^{32}P$) oligodeoxynucleotides (**Table S4**) were added and the membrane was
720 further incubated overnight at the same temperature. After three washes for 10 min at 65°C
721 with 2x SSC 0.2 % SDS, the membrane was exposed to a phosphorimager screen (KODAK)

722 and scanned with FLA-9000 Phospho Imager (Fujifilm).

723

724 **Peptidoglycan extraction and Muropeptides analysis by HPLC/HRMS**

725 Samples (1L) of *H. pylori* B128 WT strain (16h, exponential phase and 72h, "aging"
726 coccoids) and of B128 Δ*aapA1-IsoA1* pA1 strain, induced by IPTG during 6h and 16h, were
727 taken and chilled in an ice-ethanol bath. Crude murein sacculi were immediately extracted in
728 boiling sodium dodecyl sulfate (SDS 4% final). The resulting purified peptidoglycan was
729 digested overnight at 37°C in 12.5 mM sodium phosphate buffer (pH 5.6) supplemented with
730 100 UI of mutanolysin from *Streptomyces globisporus* ATCC 21553 (Sigma). The reaction
731 was stopped by heat inactivation of the enzyme and insoluble material was removed by
732 centrifugation. Soluble muropeptides were then reduced with sodium borohydride in borate
733 buffer (pH 9). After centrifugation, reduced muropeptides were diluted 20-fold in water-
734 formic acid 0.1% (v/v; solvent A). HPLC/HRMS (High Performance Liquid Chromatography
735 / High Resolution Mass Spectrometry) was performed on an Ultimate 3000 UHPLC (Ultra
736 High Performance Liquid Chromatography) system coupled to a quadrupole-Orbitrap mass
737 spectrometer (Q-Exactive Focus, Thermo Fisher Scientific). Muropeptides were separated on
738 an Hypersil Gold aQ analytical column (1.9 µm, 2.1x150 mm) at 200 µL/min, column
739 temperature at 50°C. Applied linear gradient from 0 to 12.5% acetonitrile + 0,1% (v/v) formic
740 acid (solvent B), followed by increasing to 20% B at 25 min for 5 min, hold 20% B for min
741 and additional 10 min with 100% A for column re-equilibration. Eluted muropeptides were
742 introduced into Q-Exactive instrument, operating in positive ion mode, and then were
743 analyzed in the data-dependent acquisition mode (FullMSddMS2). Data were then processed
744 with the software TraceFinder 3.3 (Thermo Fisher Scientific) for peak areas determination,
745 the relative abundance of muropeptides in each sample was calculated according to Glauner *et*
746 *al.* (23).

747

748 **Statistical analysis**

749 The Student's t test was used to determine significance of the means of the data. Error bars
750 represent the standard deviation, with * ($P < 0.05$), ** ($P < 0.01$), *** ($P < 0.001$) indicating
751 that the mean values are significantly different and NS that they are not significantly different
752 ($P > 0.05$). SEM corresponds to standard error of the mean. The two-way ANOVA multiple
753 comparisons was used to compare Northern blots bands intensities under different conditions.
754

755 References
756
757 1. Yamaguchi Y, Park J-H, & Inouye M (2011) Toxin-Antitoxin Systems in Bacteria and
758 Archaea. *Annual Review of Genetics* 45(1):61-79.
759 2. Goeders N & Van Melderen L (2014) Toxin-Antitoxin Systems as Multilevel
760 Interaction Systems. *Toxins* 6(1):304-324.
761 3. Page R & Peti W (2016) Toxin-antitoxin systems in bacterial growth arrest and
762 persistence. *Nat Chem Biol* 12(4):208-214.
763 4. Yang QE & Walsh TR (2017) Toxin–antitoxin systems and their role in disseminating
764 and maintaining antimicrobial resistance. *FEMS Microbiology Reviews* 41(3):343-353.
765 5. Helaine S*, et al.* (2014) Internalization of *Salmonella* by Macrophages Induces
766 Formation of Nonreplicating Persisters. *Science* 343(6167):204-208.
767 6. Wang X*, et al.* (2011) Antitoxin MqsA helps mediate the bacterial general stress
768 response. *Nat Chem Biol* 7(6):359-366.
769 7. Berghoff BA & Wagner EGH (2017) RNA-based regulation in type I toxin–antitoxin
770 systems and its implication for bacterial persistence. *Current Genetics*.
771 8. Harms A, Brodersen DE, Mitarai N, & Gerdes K (2018) Toxins, Targets, and
772 Triggers: An Overview of Toxin-Antitoxin Biology. *Molecular Cell*.
773 9. Harms A, Maisonneuve E, & Gerdes K (2016) Mechanisms of bacterial persistence
774 during stress and antibiotic exposure. *Science* 354(6318).
775 10. Goormaghtigh F*, et al.* (2018) Reassessing the Role of Type II Toxin-Antitoxin
776 Systems in Formation of *Escherichia coli* Type II Persister Cells. *mBio* 9(3).
777 11. Shan Y*, et al.* (2017) ATP-Dependent Persister Formation in *Escherichia coli*. *mBio*
778 8(1):e02267-02216.
779 12. Yamaoka Y (2010) Mechanisms of disease: *Helicobacter pylori* virulence factors. *Nat*
780 *Rev Gastroenterol Hepatol* 7:629–641.

781 13. Amieva M & Peek Jr RM (2016) Pathobiology of *Helicobacter pylori*–Induced
782 Gastric Cancer. *Gastroenterology* 150(1):64-78.
783 14. Loke MF, Ng CG, Vilashni Y, Lim J, & Ho B (2016) Understanding the dimorphic
784 lifestyles of human gastric pathogen *Helicobacter pylori* using the SWATH-based
785 proteomics approach. *Scientific Reports* 6:26784.
786 15. Reshetnyak VI & Reshetnyak TM (2017) Significance of dormant forms of
787 *Helicobacter pylori* in ulcerogenesis. *World Journal of Gastroenterology*
788 23(27):4867-4878.
789 16. Ayrapetyan M, Williams T, & Oliver JD (2018) The relationship between the viable
790 but nonculturable state and antibiotic persister cells. *Journal of Bacteriology*.
791 17. Brantl S & Jahn N (2015) sRNAs in bacterial type I and type III toxin-antitoxin
792 systems. *FEMS Microbiol Rev.* 39:413-427.
793 18. Masachis S & Darfeuille F (2018) Type I Toxin-Antitoxin Systems: Regulating Toxin
794 Expression via Shine-Dalgarno Sequence Sequestration and Small RNA Binding.
795 *Microbiology Spectrum* 6(4).
796 19. Sharma CM*, et al.* (2010) The primary transcriptome of the major human pathogen
797 *Helicobacter pylori*. *Nature* 464:250-255.
798 20. Arnion H*, et al.* (2017) Mechanistic insights into type I toxin antitoxin systems in
799 *Helicobacter pylori*: the importance of mRNA folding in controlling toxin expression.
800 *Nucleic Acids Research* 45(8):4782-4795.
801 21. Boneca IG*, et al.* (2008) Development of inducible systems to engineer conditional
802 mutants of essential genes of *Helicobacter pylori*. *Appl. Environ. Microbiol.*
803 74(7):2095-2102.
804 22. Stingl K, Uhlemann E-M, Schmid R, Altendorf K, & Bakker EP (2002) Energetics of
805 *Helicobacter pylori* and Its Implications for the Mechanism of Urease-Dependent
806 Acid Tolerance at pH 1. *Journal of Bacteriology* 184(11):3053-3060.

807 23. Glauner B (1988) Separation and quantification of muropeptides with high-
808 performance liquid chromatography. *Anal Biochem.* 172:451-464.
809 24. Fischer F*, et al.* (2016) A novel essential ABC transporter and the NixA permease are
810 the two sole nickel uptake systems of *Helicobacter pylori*. *PLoS Pathog* 12:e1006018.
811 25. Brantl S (2012) Bacterial type I toxin-antitoxin systems. *RNA Biology* 9(12):1488-
812 1490.
813 26. Jahn N, Brantl S, & Strahl H (2015) Against the mainstream: the membrane‐
814 associated type I toxin BsrG from *Bacillus subtilis* interferes with cell envelope
815 biosynthesis without increasing membrane permeability. *Molecular Microbiology*
816 98(4):651-666.
817 27. Brielle R, Pinel-Marie M-L, & Felden B (2016) Linking bacterial type I toxins with
818 their actions. *Current Opinion in Microbiology* 30:114-121.
819 28. Unoson C & Wagner EGH (2008) A small SOS‐induced toxin is targeted against the
820 inner membrane in *Escherichia coli*. *Molecular Microbiology* 70(1):258-270.
821 29. Sayed N, Nonin-Lecomte S, Réty S, & Felden B (2012) Functional and Structural
822 Insights of a *Staphylococcus aureus* Apoptotic-like Membrane Peptide from a Toxin-
823 Antitoxin Module. *The Journal of Biological Chemistry* 287(52):43454-43463.
824 30. Kusters JG, Gerrits MM, Van Strijp JA, & Vandenbroucke-Grauls CM (1997)
825 Coccoid forms of *Helicobacter pylori* are the morphologic manifestation of cell death.
826 *Infection and Immunity* 65(9):3672-3679.
827 31. Enroth H*, et al.* (1999) In Vitro Aging of *Helicobacter pylori*: Changes in Morphology,
828 Intracellular Composition and Surface Properties. *Helicobacter* 4(1):7-16.
829 32. Costa K*, et al.* (1999) The Morphological Transition of *Helicobacter pylori* Cells from
830 Spiral to Coccoid Is Preceded by a Substantial Modification of the Cell Wall. *J.*
831 *Bacteriol* 181(12):3710-3715.

832 33. Yang DC, Blair KM, & Salama NR (2016) Staying in Shape: the Impact of Cell Shape
833 on Bacterial Survival in Diverse Environments. *Microbiology and Molecular Biology*
834 *Reviews : MMBR* 80(1):187-203.
835 34. Bonis M, Ecobichon C, Guadagnini S, Prévost M-C, & Boneca IG (2010) A M23B
836 family metallopeptidase of *Helicobacter pylori* required for cell shape, pole formation
837 and virulence. *Molecular Microbiology* 78(4):809-819.
838 35. Chaput C*, et al.* (2006) Role of AmiA in the Morphological Transition of
839 *Helicobacter pylori* and in Immune Escape. *PLoS Pathogens* 2(9):e97.
840 36. Heller DM, Tavag M, & Hochschild A (2017) CbtA toxin of *Escherichia coli* inhibits
841 cell division and cell elongation via direct and independent interactions with FtsZ and
842 MreB. *PLoS genetics* 13(9):e1007007.
843 37. Zeng H, Guo G, Mao XH, De Tong W, & Zou QM (2008) Proteomic Insights into
844 *Helicobacter pylori* Coccoid Forms Under Oxidative Stress. *Current Microbiology*
845 57(4):281.
846 38. Müller P*, et al.* (2016) A multistress responsive type I toxin-antitoxin system:
847 bsrE/SR5 from the *B. subtilis* chromosome. *RNA Biology* 13(5):511-523.
848 39. Cellini L (2014) *Helicobacter pylori*: A chameleon-like approach to life. *World*
849 *Journal of Gastroenterology* 20(19):5575-5582.
850 40. Segal ED, Falkow S, & Tompkins LS (1996) *Helicobacter pylori* attachment to gastric
851 cells induces cytoskeletal rearrangements and tyrosine phosphorylation of host cell
852 proteins. *Proceedings of the National Academy of Sciences of the United States of*
853 *America* 93(3):1259-1264.
854 41. Goldstein NS (2002) Chronic Inactive Gastritis and Coccoid *Helicobacter pylori* in
855 Patients Treated for Gastroesophageal Reflux Disease or With H pylori Eradication
856 Therapy. *American Journal of Clinical Pathology* 118(5):719-726.

857 42. Nagai S, *et al.* (2007) Role of Peyer's patches in the induction of *Helicobacter pylori*-
858 induced gastritis. *Proceedings of the National Academy of Sciences of the United*
859 *States of America* 104(21):8971-8976.
860 43. Cellini L, *et al.* (1994) Coccoid *Helicobacter pylori* not culturable *in vitro* reverts in
861 mice. *Microbiology and Immunology* 38(11):843-850.
862 44. Butcher LD, den Hartog G, Ernst PB, & Crowe SE (2017) Oxidative Stress Resulting
863 From *Helicobacter pylori* Infection Contributes to Gastric Carcinogenesis. *Cellular*
864 *and Molecular Gastroenterology and Hepatology* 3(3):316-322.
865 45. Ayrapetyan M, Williams TC, & Oliver JD (2015) Bridging the gap between viable but
866 non-culturable and antibiotic persistent bacteria. *Trends in microbiology* 23(1):7-13.
867 46. Rotem E, *et al.* (2010) Regulation of phenotypic variability by a threshold-based
868 mechanism underlies bacterial persistence. *Proceedings of the National Academy of*
869 *Sciences of the United States of America* 107(28):12541-12546.
870 47. Farnbacher M, *et al.* (2010) Sequencing, annotation and comparative genome analysis
871 of the gerbil-adapted *Helicobacter pylori* strain B8. *BMC Genom.* 11:335.: doi:
872 10.1186/1471-2164-1111-1335.
873 48. McClain MS, Shaffer CL, Israel DA, Peek RMJ, & Cover TL (2009) Genome
874 sequence analysis of *Helicobacter pylori* strains associated with gastric ulceration and
875 gastric cancer. *BMC Genom.* 10:3:doi: 10.1186/1471-2164-1110-1183.
876 49. Debowski AW, *et al.* (2012) Xer-cise in *Helicobacter pylori*: one-step transformation
877 for the construction of markerless gene deletions. *Helicobacter* 17:435-443.
878 50. Kutter S, *et al.* (2008) Protein Subassemblies of the *Helicobacter pylori* Cag Type IV
879 Secretion System Revealed by Localization and Interaction Studies. *Journal of*
880 *Bacteriology* 190(6):2161-2171.
881 51. El Ghachi M, *et al.* (2011) Characterization of the elongasome core PBP2: MreC
882 complex of *Helicobacter pylori*. *Molecular Microbiology* 82(1):68-86.

883 52. Muller C*, et al.* (2011) Hierarchical regulation of the NikR-mediated nickel response
884 in *Helicobacter pylori*. *Nucleic Acids Res.* 39:7564-7575.
885 53. Corbinais C, Mathieu A, Kortulewski T, Radicella JP, & Marsin S (2016) Following
886 transforming DNA in *Helicobacter pylori* from uptake to expression. *Mol Microbiol*
887 101(6):1039-1053.
888 54. Miller JH (1992) *A short Course in Bacterial Genetics : A laboratory manual and*
889 *handbook for Escherichia coli and related bacteria. Cold Spring Harbor, N. Y* (Cold
890 Spring Harbor Laboratory).

891

Figure 1

A

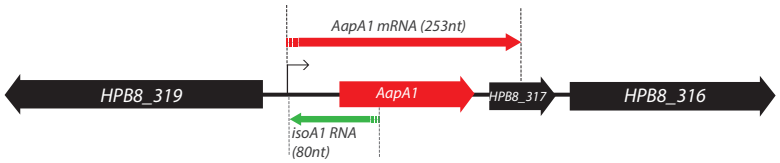
AapA1 mRNA (253nt)
HPB8_319
AapA1
HPB8_317
HPB8_316
isoA1 RNA
(80nt)

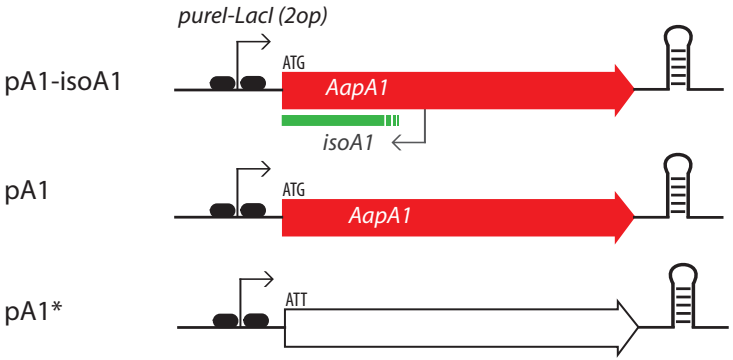
purel-LacI (2op)
pA1-isoA1
ATG
AapA1
isoA1
pA1
ATG
AapA1
pA1*
ATT

B

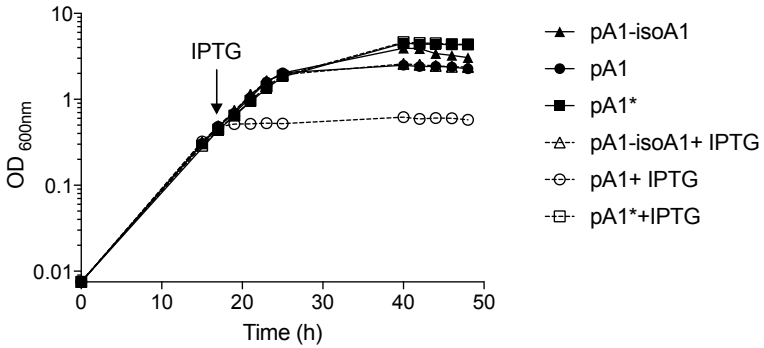
IPTG
OD 600nm
10
1
0.1
0.01
0
10
20
30
40
50
Time (h)
pA1-isoA1
pA1
pA1*
pA1-isoA1+ IPTG
pA1+ IPTG
pA1*+IPTG

C

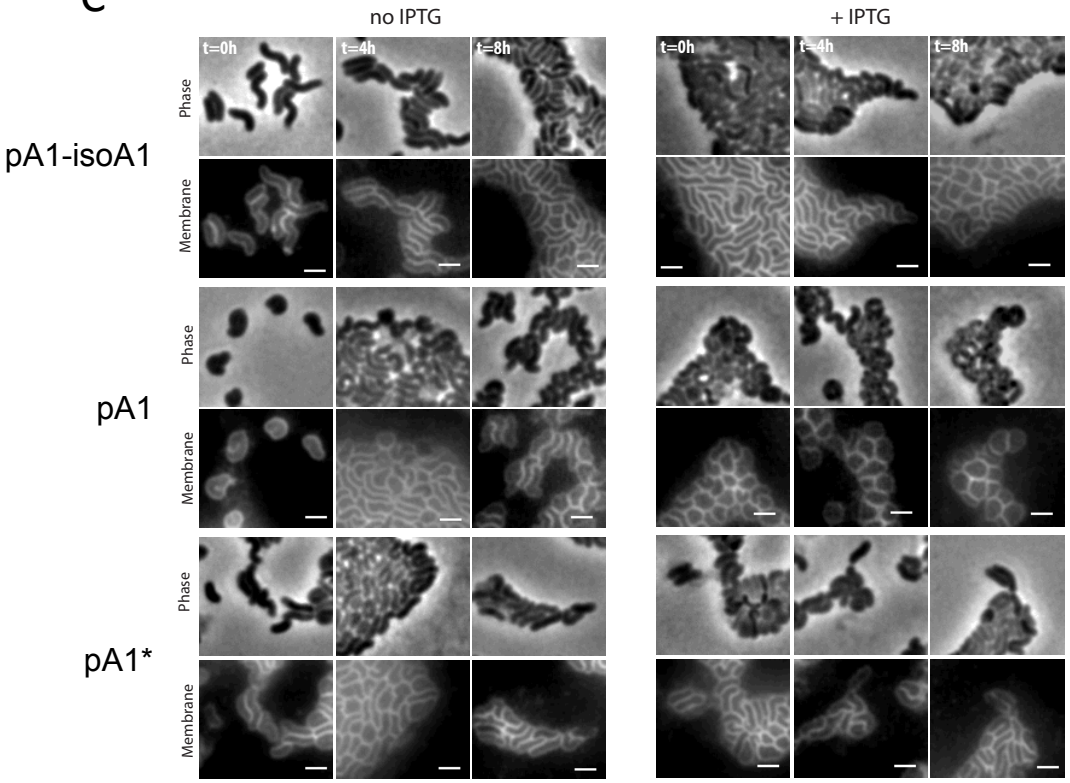
no IPTG
+ IPTG
t=0h
t=4h
t=8h
Phase
Membrane
pA1-isoA1
pA1
pA1*

Figure 2

A

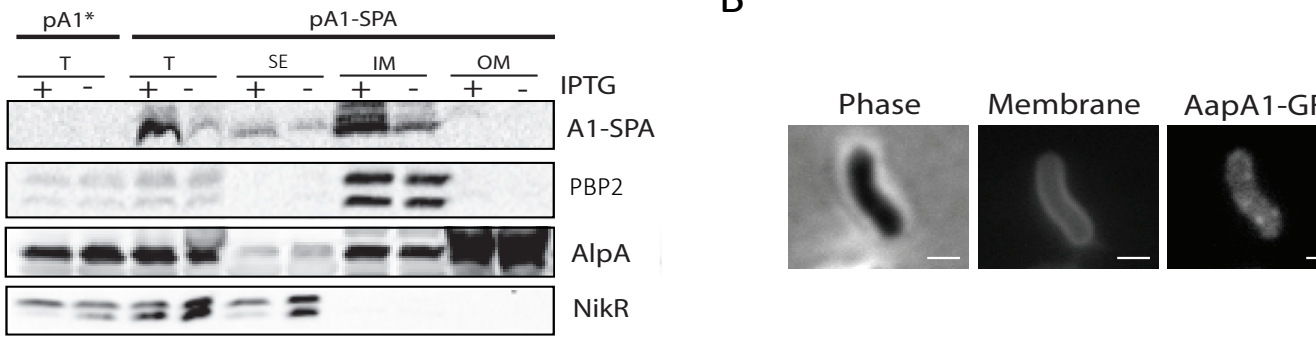

B

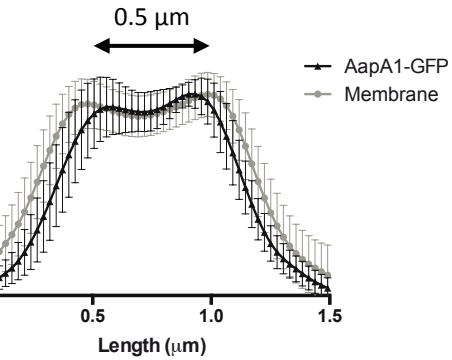

C

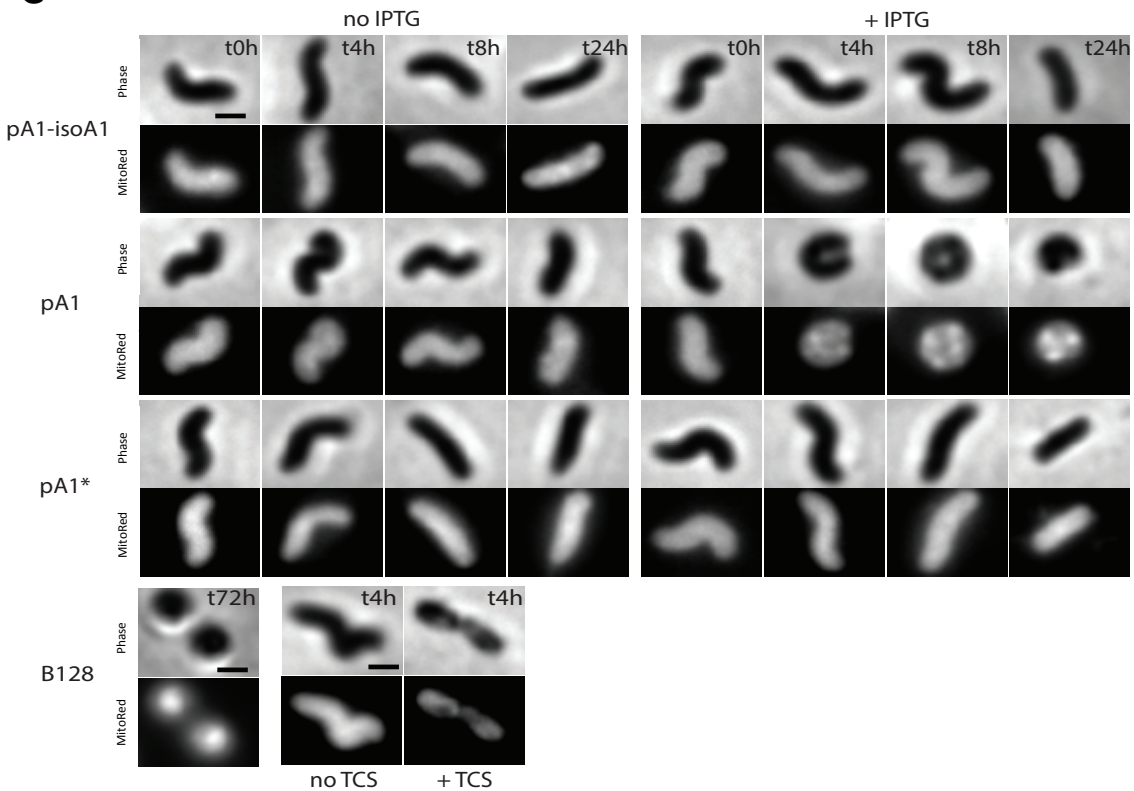

D

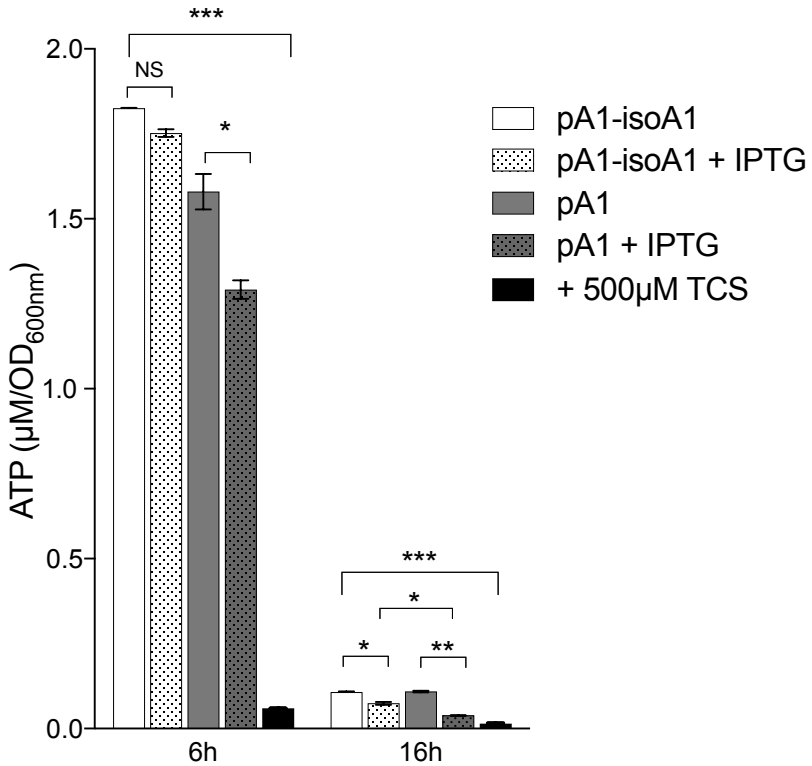

Figure 3

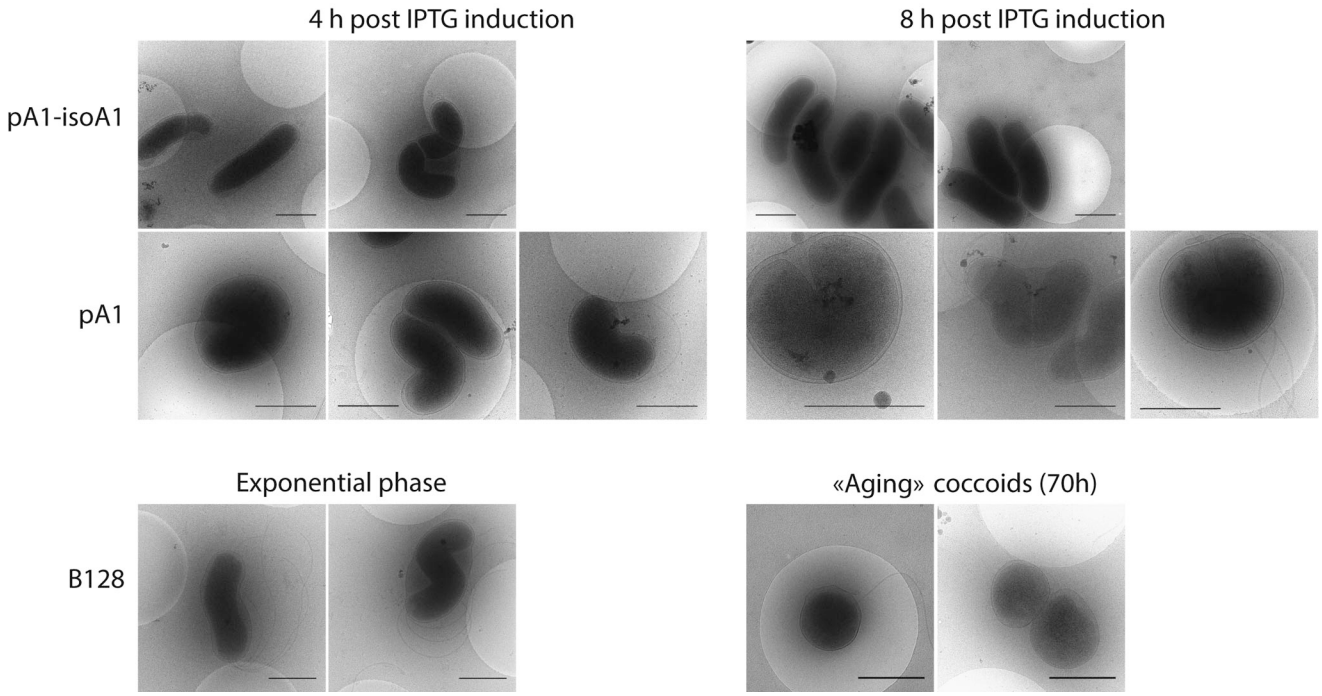
4 h post IPTG induction
8 h post IPTG induction
pA1-isoA1
pA1
Exponential phase
«Aging» coccoids (70h)
B128

Figure 4

A

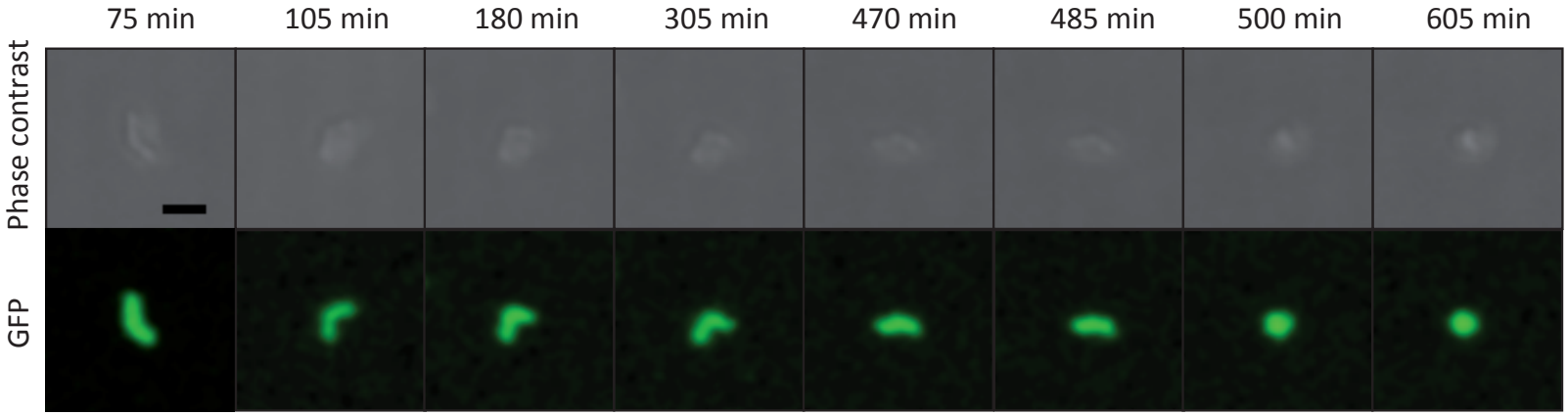

B

	Time before «bending» phenotype (min)	Time before «pseudo-coccoid» phenotype (min)	Time before «donut» phenotype (min)	Maximum length before morphological change (µm)
Number of cells	49	37	21	63
Median	180	280	420	3.58
Mean ± SEM	185 ± 8.0	277 ± 16	420 ± 25.2	3.48 ± 0.08

Figure 5

A.

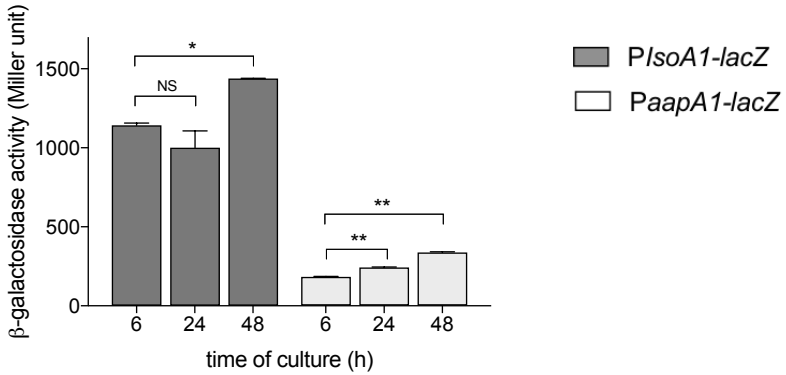

B.

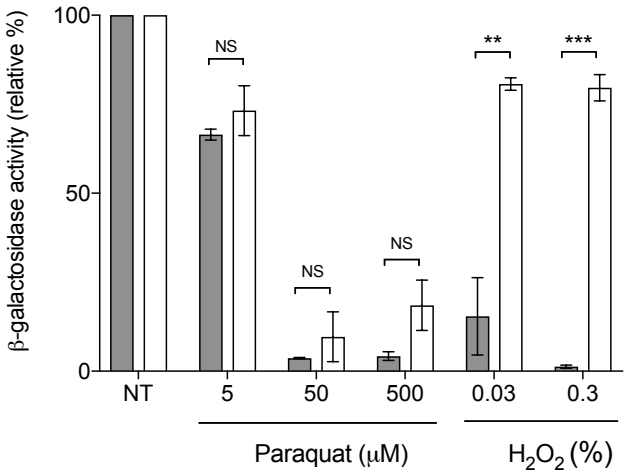

C.

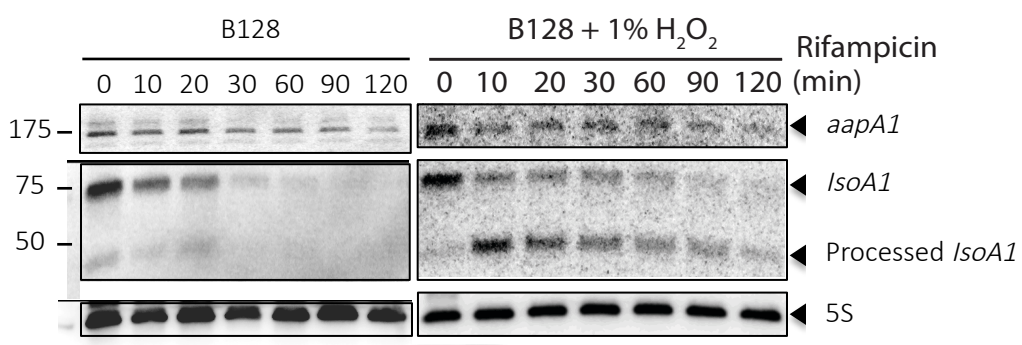
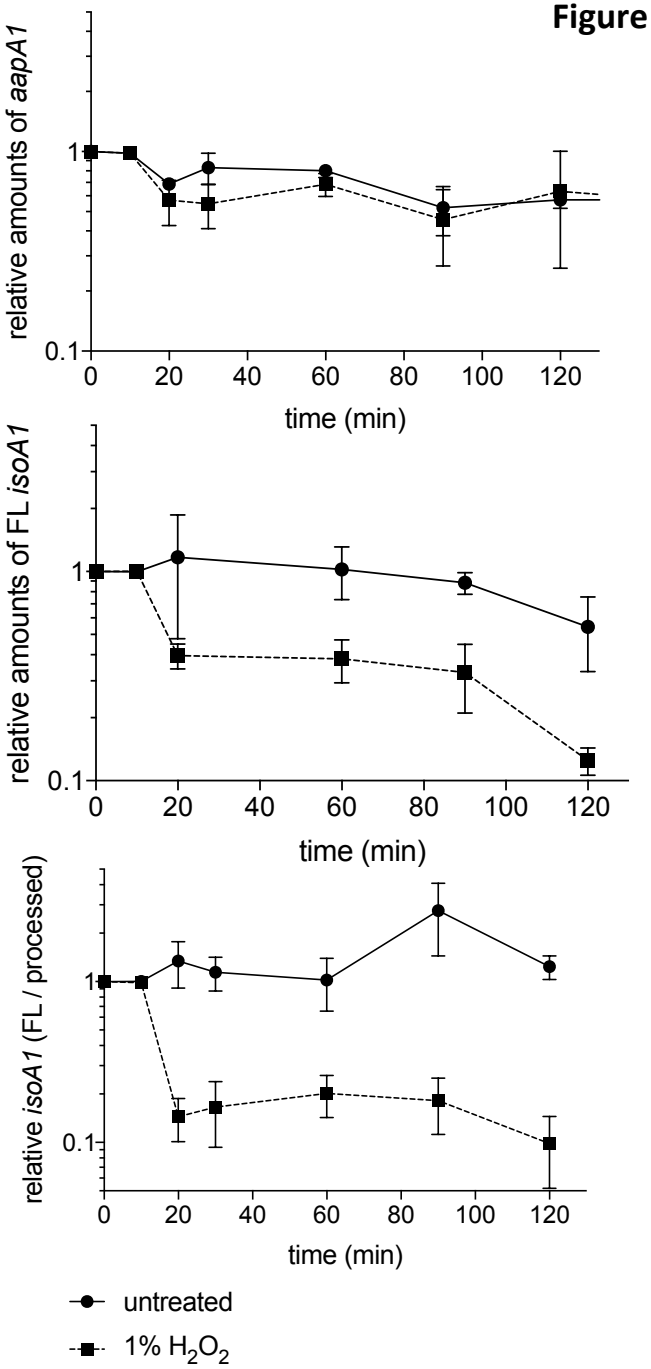
D.